Materials and Design 194 (2020) 108925

Contents lists available at ScienceDirect

Materials and Design

journal homepage: www.elsevier.com/locate/matdes

Inverse estimation approach for elastoplastic properties using the load-displacement curve and pile-up topography of a single Berkovich indentation

Kenta Goto [a,*], Ikumu Watanabe [b], Takahito Ohmura [b]

[a] International Center for Young Scientists, National Institute for Materials Science, 1-2-1 Sengen, Tsukuba 305-0047, Japan
[b] Research Center for Structural Materials, National Institute for Materials Science, 1-2-1 Sengen, Tsukuba 305-0047, Japan

HIGHLIGHTS

- Elastoplastic properties were derived from the mechanical response of an indentation test
- An algorithm based on equivalent energy model and limit-analysis was proposed
- The coefficients for the algorithm were determined using finite element analysis
- The inverse estimation of elastoplastic properties based on the proposed model was highly correlated with the tensile tests

GRAPHICAL ABSTRACT

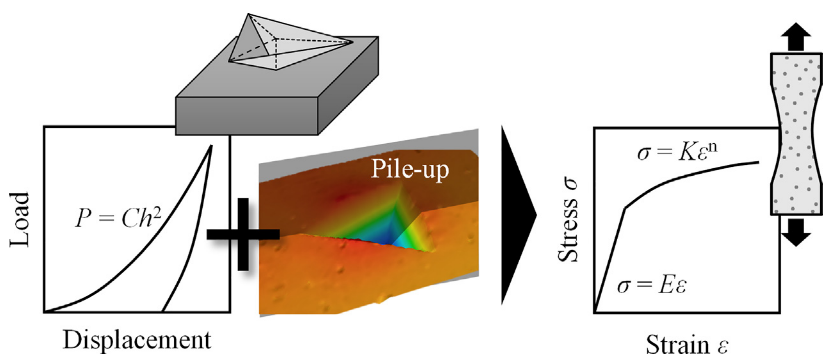

ARTICLE INFO

Article history:
Received 12 February 2020
Received in revised form 22 June 2020
Accepted 24 June 2020
Available online 29 June 2020

Keywords:
Elastic-plastic material
Finite elements
Mechanical testing
Indentation
Inverse analysis

ABSTRACT

An approach for the inverse estimation of the elastoplastic properties from a single indentation with a Berkovich indenter was developed. The relationship between the load-displacement and stress-strain curves was derived based on the equivalent energy principle, while an approximate equation for pile-up height was determined using elastic and plastic limits. The approach proposed in this study estimates the yield stress and strain-hardening exponent from hardness and pile-up height obtained from a single indentation based on these fundamental equations. The coefficients in the equations were determined in a parametric study using finite element analyses. The accuracy of the inverse estimation technique was confirmed using aluminum alloy and stainless steel samples and reference tensile testing.

1. Introduction

Indentation testing is widely implemented in the field of engineering due to its simplicity. It is used to evaluate the mechanical properties of a material, particularly hardness. An indentation test simultaneously records the load (P) and displacement (h) (Fig. 1a), allowing the calculation of elastic modulus and hardness [1], residual stress [2,3], creep [4,5], phase transition [6], and the onset of plastic deformation [7].

In a bulk material, the reduced elastic modulus (E_r) and indentation hardness (H_{it}) are calculated from the load-displacement curve according to the Oliver-Pharr (OP) method [8] as follows:

* Corresponding author.
E-mail address: GOTO.Kenta@nims.go.jp (K. Goto).

https://doi.org/10.1016/j.matdes.2020.108925
0264-1275/

$$E_r = \frac{S\sqrt{\pi}}{2\sqrt{A_{(h_c)}}}, \tag{1}$$

$$H_{it} = \frac{P_{max}}{A_{(h_c)}}, \tag{2}$$

$$\frac{1}{E_r} = \frac{1-\nu_i^2}{E_i} + \frac{1-\nu_s^2}{E_s} = \frac{1-\nu_i^2}{E_i} + \frac{1}{M}, \tag{3}$$

where S is contact stiffness, h_c is contact depth, P_{max} is the maximum load and $A_{(hc)}$ is contact area at $h = h_c$. E and ν are Young's modulus and Poisson's ratio, respectively, where subscripts i and s represent the indenter and sample, respectively. The authors define indentation modulus (M) as $E_s/(1\text{-}\nu_s^2)$.

The stress-strain curve obtained from a uniaxial tensile test (Fig. 1b) provides the essential information regarding mechanical properties required in the design and evaluation of structural materials. The simplest approximation of the stress-strain curve uses Young's modulus (E), a strain hardening coefficient (K), and a strain hardening exponent (n), as given in Eqs. (4) and (5):

$$\sigma = E\varepsilon \text{ at } \sigma \le \sigma_y, \tag{4}$$

$$\sigma = K\varepsilon^n \text{ at } \sigma \ge \sigma_y, \tag{5}$$

where σ and ε represent stress and strain, respectively, and σ_y is yield stress. Eqs. (4) and (5) are continuous at the yield point ($\sigma = \sigma_y$), and thus $K = E^n\sigma_y^{1\text{-}n}$. Therefore, Eq. (5) is replaced by Eq. (6), as follows:

$$\sigma = E^n\sigma_y^{1-n}\varepsilon^n. \tag{6}$$

Many techniques have been proposed to inversely estimate the stress-strain relationship from the results of an indentation test, and these techniques use either spherical or pyramidal indenters. Inverse estimation techniques using spherical indenters [9–12] generate a continuous stress-strain curve from a single indentation as the strain field under the indenter changes with increasing indentation depth. However, the indenter tip radius must be adjusted according to the area being evaluated. Pyramidal indenters such as conical, Berkovich, and Vickers indenters similarly have a geometry independent on depth. Most of the techniques using pyramidal indenters determine the elastic modulus using Eqs. (1) and (3). The dual indenter technique [13–22] is a common inverse estimation technique applied to pyramidal indenters. It estimates the yield stress and strain hardening exponent from two load-displacement curves, each obtained using indenters with different tip angles, as the yield stress and strain hardening exponent of an unknown sample cannot be determined from a single load-displacement curve [23–25]. Numerous studies [15,17–19,26] have used dimensionless polynomial functions based on Π theory, where the coefficients for the functions were determined using finite element analysis. A technique proposed by Ogasawara et al. [16] was based on limit analysis that considered the elastic and plastic limits. Chen and Cai [13] proposed a relationship between the load-displacement curve and elastoplastic properties based on an equivalent energy principle and Johnson's cavity model [27]. Furthermore, the effectiveness of these dual indenter techniques has been compared by Guelorget et al. [28] and Kang et al. [29].

The stress-strain relationship can be estimated from a single indentation result by analyzing not only a load-displacement curve but also the three-dimensional pile-up topography after indentation using confocal microscopy or atomic force microscopy (AFM). Goto et al. [30] demonstrated that the residual pile-up height is related to the yield stress and strain hardening exponent as well as the load-displacement curve in finite element analysis, where the residual pile-up height was strongly dependent on the strain hardening exponent. The sensitivity

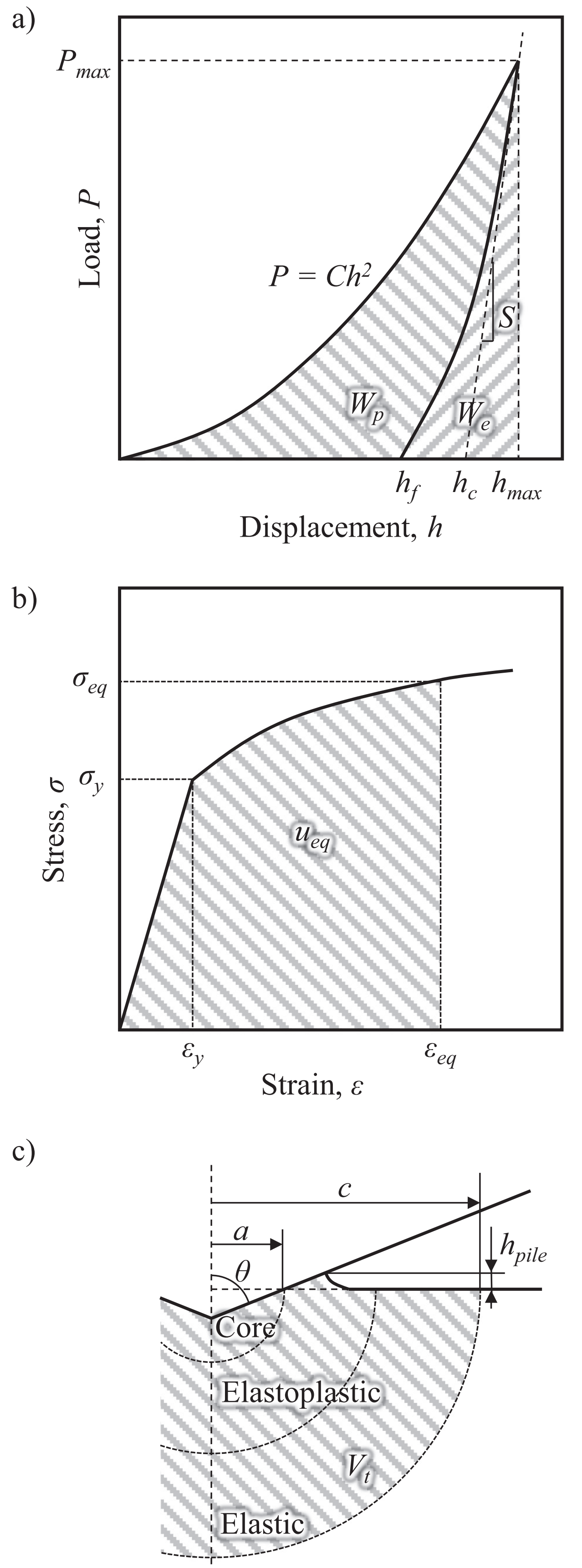

Fig. 1. Schematic of the (a) load-displacement curve, (b) stress-strain curve and (c) deformation under a conical indenter based on Johnson's cavity model.

of the pile-up topography was further investigated by Meng et al. [31]. The load-displacement curve and pile-up topography from a single indentation test were used to estimate stress-strain curves, as shown in Goto et al. [30], Meng et al. [32], and Bolzon et al. [33]. These studies performed a large number of indentation simulation iterations to obtain a simulation that accurately reflects the experimental result. However, these iterations of finite element analysis are time-consuming.

This study aimed to establish a relationship between elastoplastic properties and indentation results for an inverse estimation based on the load-displacement curve and pile-up topography of a single indentation. A Berkovich indenter was chosen for its frequent use in previous studies involving instrumented indentation. The study focused on modeling and formulation, and determined the modeling coefficients using a finite element analysis parametric study. The proposed model was validated by conducting further inverse estimations.

2. Inverse estimation model

2.1. Load-displacement curve

The relationship between the load-displacement curve and elastoplastic properties was established using the equivalent energy model [13]. An indentation causes elastoplastic deformation of the sample material beneath the indenter. The total strain energy (U_t) in the deformed region (V_t) is obtained by integrating strain energy density (u) at each point (Fig. 1c),

$$U_t = \int_{V_t} u dV. \tag{7}$$

The equivalent strain energy (u_{eq}) was defined as a volumetrically averaged value according to Eq. (8) as follows:

$$u_{eq} = \frac{\int_{V_t} u dV}{V_t}. \tag{8}$$

u_{eq} was decomposed at the yield point into two components, namely the elastic ($u_{eq,e}$) and elastoplastic ($u_{eq,ep}$) components (Fig. 1b). According to the power law in the elastoplastic region (Eq. (5)), u_{eq} is represented in terms of E, K, and n, as follows:

$$u_{eq,e} = \int_0^{\varepsilon_y} \sigma d\varepsilon = \frac{E\varepsilon_y^2}{2} = \frac{K\varepsilon_y^{1+n}}{2}, \tag{9}$$

$$u_{eq,ep} = \int_{\varepsilon_y}^{\varepsilon_{eq}} \sigma d\varepsilon = \frac{K}{1+n}\left(\varepsilon_{eq}^{1+n} - \varepsilon_y^{1+n}\right), \tag{10}$$

$$\therefore u_{eq} = u_{eq,e} + u_{eq,ep} = \frac{K}{1+n}\left(\varepsilon_{eq}^{1+n} - \frac{1-n}{2}\varepsilon_y^{1+n}\right) \approx \frac{K\varepsilon_{eq}^{1+n}}{1+n}, \tag{11}$$

where ε_y and ε_{eq} are the yield strain ($=\sigma_y/E$) and strain at $u = u_{eq}$, respectively. It was assumed that ε_y is substantially smaller than ε_{eq}:

$$\frac{1-n}{2}\left(\frac{\varepsilon_y}{\varepsilon_{eq}}\right)^{1+n} \ll 1. \tag{12}$$

Atkins and Tabor [34] proposed representative plastic strain (ε_r), which was the strain attributed to plastic deformation induced by indentation. The representative plastic strain has been determined in previous studies [14,35], most of which use Eq. (13) to approximate the relationship between ε_r and indenter tip angle (θ), as follows:

$$\varepsilon_r = B_{e1} \cot\theta, \tag{13}$$

where B_{e1} is constant. It may be assumed that ε_{eq} has a similar relationship:

$$\varepsilon_{eq} = k_{e1} \cot\theta, \tag{14}$$

where k_{e1} is also a constant. The equivalent energy model assumes that the form of the indenter is conical, but the contact area of a conical indenter is equivalent to a Berkovich indenter when $\theta = 70.3°$.

Deformed volume (V_t) may be estimated using Johnson's cavity model [13], which assumes that the deformed region is hemispherical and consists of a core, elastoplastic, and elastic regions (Fig. 1c).

$$V_t = \frac{2}{3}\pi c^3 = \frac{2}{3}\pi\left(f_{e1(\varepsilon_y,n,\theta)}a\right)^3 = \frac{2}{3}\pi\left(f_{e1(\varepsilon_y,n,\theta)}h_{max}\tan\theta\right)^3, \tag{15}$$

where a and c are the radii of the core and elastic regions, respectively. $f_{e1} = c/a$ is a function of the elastoplastic properties and the tip angle, but the elastic modulus has a minor effect on f_{e1} (see Section 3). Thus, the total strain energy U_t was derived from Eqs. (8), (11), (14), and (15) to give Eq. (16), as follows:

$$U_t = u_{eq}V_t = \frac{2}{3}\pi\frac{K}{1+n}(k_{e1}\cot\theta)^{1+n}\left(f_{e1(\varepsilon_y,n,\theta)}h_{max}\tan\theta\right)^3. \tag{16}$$

The total strain energy is equal to the total indentation work (W_t), where $W_t = W_e + W_p$, as follows:

$$U_t = W_t. \tag{17}$$

W_t is calculated by integrating the indentation load (P) with the displacement (h) during loading:

$$W_t = \int_0^{h_{max}} P dh = \frac{1}{3}Ch_{max}^3. \tag{18}$$

Here, the load-displacement curve was approximated by a parabolic curve:

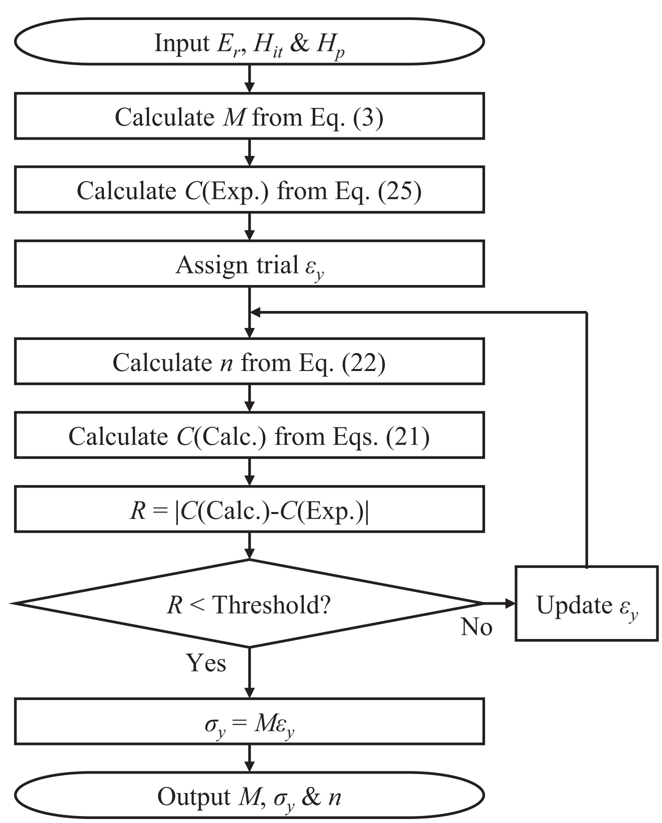

Fig. 2. Algorithm for the inverse estimation of E_r, H_{it}, and H_p.

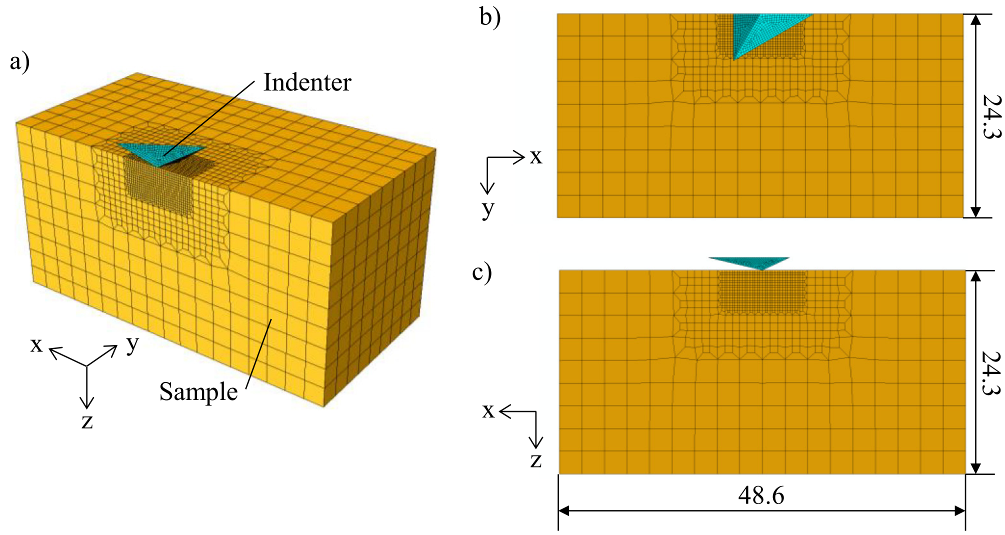

Fig. 3. Analytical model of a Berkovich indenter shown from the (a) perspective, (b) top and (c) side views.

$$P = Ch^2. \tag{19}$$

The curvature of the loading curve (C) was correlated to the elastoplastic parameters M, σ_y ($= M \times \varepsilon_y$) and n using Eqs. (16)–(18):

$$\frac{2}{3}\pi\frac{K}{1+n}(k_{e1}\cot\theta)^{1+n}\left(f_{e1(\varepsilon_y,n,\theta)}h_{max}\tan\theta\right)^3 = \frac{1}{3}Ch_{max}^3, \tag{20}$$

$$\therefore C = \frac{2\pi k_{e1}^{1+n}\left(f_{e1(\varepsilon_y,n,\theta)}\right)^3 M\varepsilon_y^{1-n}\tan^{2-n}\theta}{1+n}. \tag{21}$$

Young's modulus (E) was replaced by the indentation modulus (M) because the model was under plain-strain condition.

2.2. Pile-up topography

Pile-up occurs due to isovolumetric plastic flow parallel to the indenter surface when the strain is concentrated directly below the indenter. Therefore, the maximum pile-up height occurs when $\varepsilon_y = n = 0$. Under elastic deformation, i.e., $\varepsilon_y = \infty$ or $n = 1$, the residual pile-up height (h_{pile}) must be 0 because the indented surface will return to its original form (i.e. no indentation) upon removal of the indenter. Goto et al. [30] demonstrated that the residual pile-up height decreases with an increase in ε_y and n.

The normalized residual pile-up height (H_p) is given in Eq. (22), as follows:

$$H_p = h_{pile}/h_{max} = k_{p1}\exp(-k_{p2}\varepsilon_y - k_{p3}n), \tag{22}$$

where k_{p1}, k_{p2}, and k_{p3} are constants.

Table 1
The input elastoplastic properties for the finite element analyses in the parametric study (120 cases).

Property	Value
M [GPa]	40, 120, 200, 280
ε_y	5×10^{-4}, 2.5×10^{-3}, 5×10^{-3}, 7.5×10^{-3}, 1×10^{-2}
n	0.0, 0.1, 0.2, 0.3, 0.4, 0.5

2.3. Extension to hardness

The OP method evaluates the indentation hardness (H_{it}) in addition to the reduced elastic modulus, as given in Eq. (2). Commercial software packages calculate not C but the hardness value (H_{it}) from the load-displacement results. Therefore, H_{it} is preferable to C for the calculation of the elastoplastic properties.

The OP method calculates contact depth according to Eq. (23):

$$h_c = h_{max} - \frac{eP_{max}}{S}, \tag{23}$$

where e depends on indenter geometry and $e = 0.75$ for pyramidal indenters. The ideal Berkovich indenter has a relationship described by Eq. (24):

$$A_{(h)} = C_0h^2, \tag{24}$$

where $C_0 = 24.56$. Eqs. (2), (19), (23), and (24) is combined to calculate C from E_r and H_{it} according to Eq. (25), as follows:

$$C = H_{it}C_0\left(\frac{h_c}{h_{max}}\right)^2 = H_{it}C_0\left(\frac{2E_r}{2E_r + \varepsilon H_{it}\sqrt{C_0\pi}}\right)^2. \tag{25}$$

Although the OP method is widely accepted for the calculation of elastic modulus and hardness, it causes the error of contact area when pile-up occurs [36,37] (See 3.4. Discussion). The error is remarkable for materials with small strain hardening exponent. If different algorithm is used for the calculation of hardness, Eq. (25) should be modified according to the used algorithm.

2.4. Inverse estimation algorithm

The elastoplastic properties, including indentation modulus (M), yield stress (σ_y), and strain hardening exponent (n), are estimated from the indentation results, specifically the reduced elastic modulus (E_r), indentation hardness (H_{it}), and normalized pile-up height (H_p).

The inverse estimation algorithm is based on the E_r, H_{it} and H_p results (Fig. 2). M is calculated from E_r, and the assigned trial yield strain (ε_y) is used to calculate n from H_p. The ε_y value is optimized according to residual error between the calculated and experimental C values. Iterations are discontinued once a sufficiently low error is achieved, and σ_y and

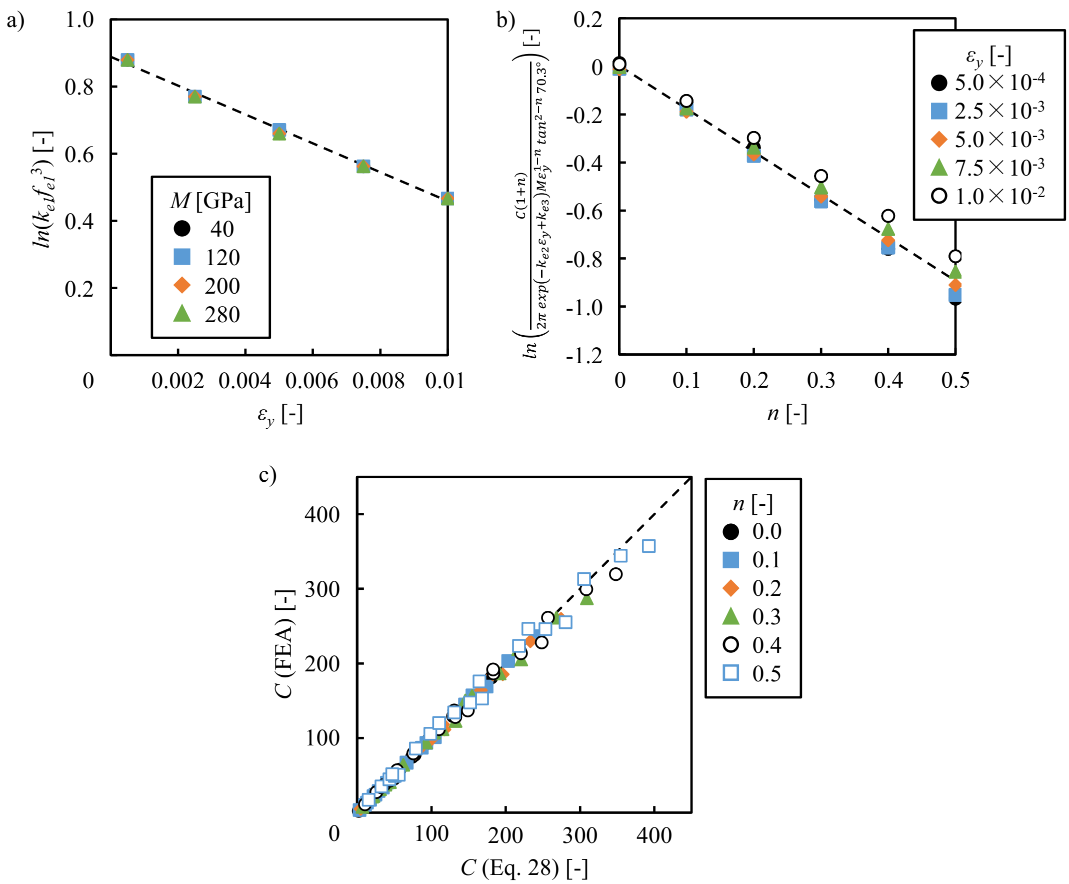

Fig. 4. Determination of the coefficients for C, specifically (a) the relationship between $k_{e1}f_{e1}^3$ with ε_y at $n = 0$, which was independent of elastic modulus; (b) the relationship between the left term in Eq. (29) and n; and (c) the high correlation between the C values calculated using Eq. (28) and finite element analyses (FEA).

Table 2
The coefficients determined using finite element analyses.

Coefficient	k_{e1}	k_{e2}	k_{e3}	k_{p1}	k_{p2}	k_{p3}
Value	0.1702	42.94	0.8881	0.4162	130.4	7.469

n are determined according to the trial ε_y. The C value may alternatively be used instead of H_{it} for this estimation.

3. Determination of coefficients using finite element analysis

3.1. Analytical model

A finite element model of a Berkovich indentation is illustrated in Fig. 3, generated using a commercial finite element analysis package (ABAQUS 6.14). The dimensions of the sample sections were $48.6 \times 24.3 \times 24.3$, and the smallest element size was 0.3. The simulated sample was meshed with an 8-node hexahedral element (C3D8), and the Berkovich indenter was assumed to be rigid and was meshed with 3- and 4-node rigid elements. The model included a total of 15,805 nodes and 14,543 elements. Bucaille et al. [14] found that the friction between the indenter and sample had a minor effect at $\theta > 60°$, but an increase in the friction coefficient caused an increase in the indentation load and a decrease in the pile-up height. A friction coefficient of 0.2 was selected for the present study as well as Chen and Cai [13]. The indenter was displaced by 1 in the loading step and returned to its initial position in the subsequent unloading step. The indentation load and pile-up height were multiplied by a factor of 1.2 and 1.3, respectively, which was determined by applying forward analysis to an experimental tensile test.

A wide variety of input elastoplastic properties were included in the sample set to consider a diverse range of metals [38] (Table 1).

3.2. Coefficients of the load-displacement curve

A strain hardening exponent of $n = 0$ allows the adaption of Eq. (21) to Eq. (26), as follows:

$$k_{e1}\left(f_{e1(\varepsilon_y,0,\theta)}\right)^3 = \frac{C}{2\pi M\varepsilon_y \tan^2\theta}. \tag{26}$$

The tip angle of the conical indenter (θ) is 70.3° to provide the same contact area as a Berkovich indenter. The $\ln\{k_{e1}(f_{e1(\varepsilon y,0,70.3°)})^3\}$ term is dependent on ε_y at $n = 0$ (Fig. 4a), indicative of the linear relationship with ε_y, which was independent of the reduced elastic modulus (M). This was approximated by Eq. (27):

$$ln\left\{k_{e1}\left(f_{e1(\varepsilon_y,0,70.3\circ)}\right)^3\right\} = -k_{e2}\varepsilon_y + k_{e3}, \tag{27}$$

where k_{e2} and k_{e3} are constants.

Assuming f_{e1} is independent of n, Eq. (28) is obtained by substituting Eq. (27) into Eq. (21), as follows:

$$C = \frac{2\pi k_{e1}^n \exp\left(-k_{e2}\varepsilon_y + k_{e3}\right) M\varepsilon_y^{1-n} \tan^{2-n}70.3\circ}{1+n}. \tag{28}$$

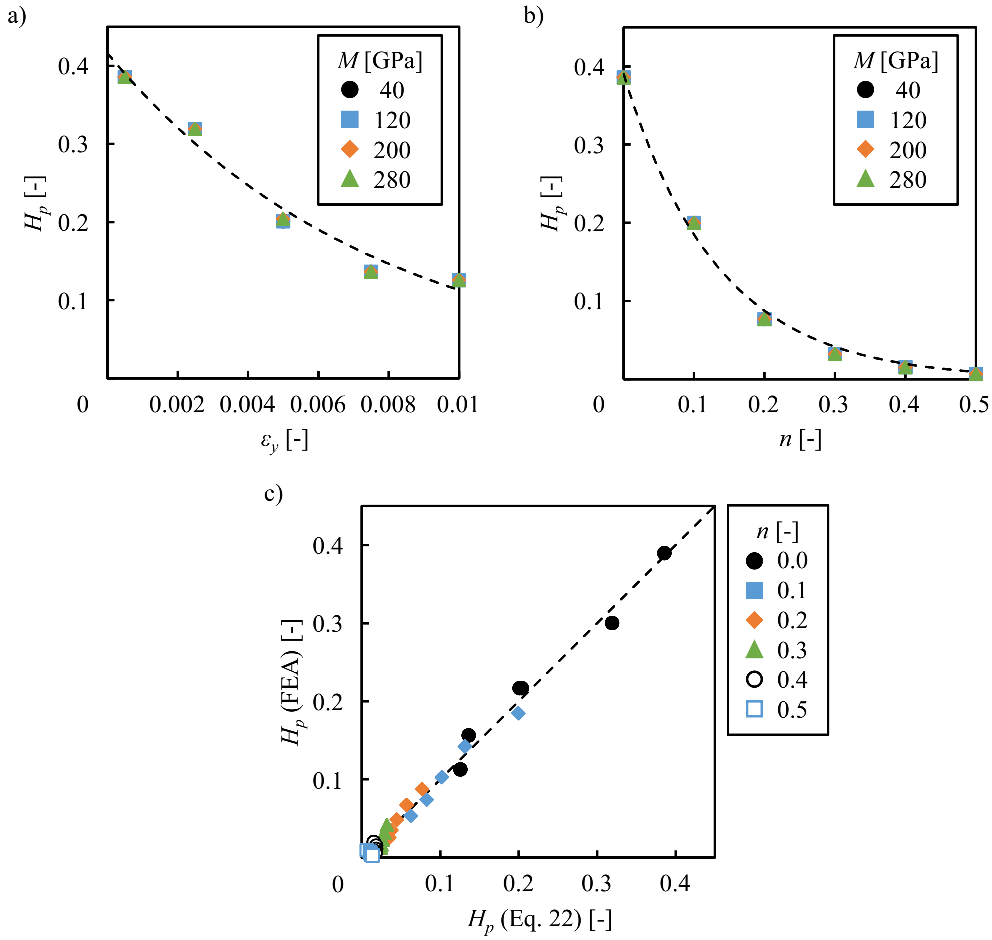

Fig. 5. The relationship between H_p and (a) ε_y at a fixed n value of 0 and (b) n at a fixed ε_y value of 5×10^{-4}, and (c) the high correlation between the H_p values calculated using Eq. (22) and finite element analysis (FEA).

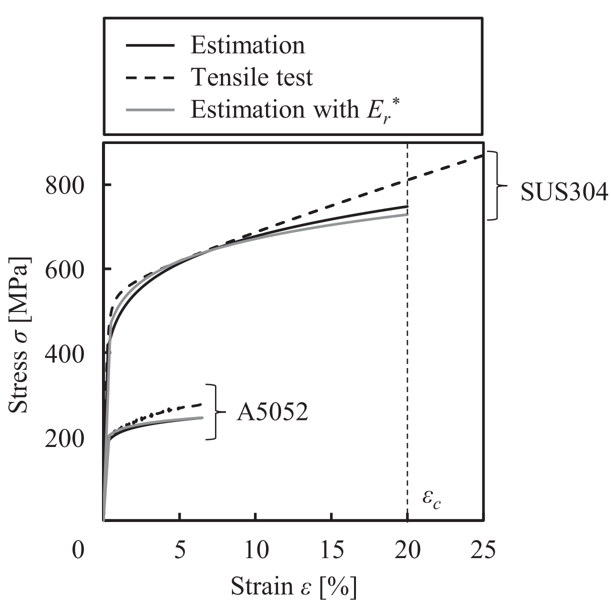

Fig. 6. The true stress-strain curves of the aluminum alloy (A5052) and stainless steel (SUS304) estimated from the indentation results (E_r, H_{it}, and H_p) and measured in the tensile tests. The estimated curves of stainless steel are given until ε reached 20%, as the upper limit of strain (ε_c) for an estimated curve is 20% at $\theta = 70.3°$. The estimation results for a reduced E_r ($E_r^* = E_r/1.3$) are given in gray.

Eq. (28) can be rearranged to give Eq. (29):

$$ln \frac{C(1+n)}{2\pi exp(-k_{e2}\varepsilon_y + k_{e3}) M \varepsilon_y^{1-n} \, tan^{2-n} 70.3^{\circ}} = n ln k_{e1}. \quad (29)$$

Eq. (29) was validated (Fig. 4b) and k_{e1} was determined using the least square method. The values of k_{e1}, k_{e2} and k_{e3} are given in Table 2.

The C values calculated using Eq. (28) were plotted against those obtained from the finite element analyses (Fig. 4c) to demonstrate that Eq. (28) provided an accurate estimation. The maximum error between the C values calculated using Eq. (28) and the finite element analyses was 36 GPa.

3.3. Coefficients of pile-up topography

The H_p value exponentially decreased with increasing ε_y at a fixed n value of 0 (Fig. 5a) and increasing n at a fixed ε_y value of 5×10^{-4} (Fig. 5b), but was independent of M, as expected from the findings in Section 2. The coefficients in Eq. (22) were determined using the least square method (Table 2).

The H_p values calculated using Eq. (22) were plotted against those obtained from the finite element analyses (Fig. 5c) to reveal that Eq. (22) expressed the dependence of H_p across a wide range of elastoplastic properties. The maximum error between the H_p values calculated using Eq. (22) and the finite element analyses was 0.02.

3.4. Discussion

The B_{e1} coefficient for the representative plastic strain (ε_r) in Eq. (13) depends on the definition of ε_r, and was found to be 0.0319 and 0.105 by Ogasawara et al. [35] and Bucaille et al. [14], respectively. However, ε_{eq} includes elastic strain in addition to plastic strain, and thus the coefficient k_{e1} in Eq. (14) is larger than B_{e1}. The k_{e1} value in this study was similar to the findings of Chen et al. [13].

The ratio of c to a (f_{e1}) determines the volume affecting the load-displacement curve. f_{e1} was calculated from Eq. (27) to give Eq. (30), as follows:

$$f_{e1} = \left\{ \frac{1}{k_{e1}} exp\left(-k_{e2}\varepsilon_y + k_{e3}\right) \right\}^{\frac{1}{3}}, \tag{30}$$

where f_{e1} has a maximum value of 2.409 at $\varepsilon_y = 5 \times 10^{-4}$ and a minimum of 2.103 at $\varepsilon_y = 1 \times 10^{-2}$. The elastoplastic boundaries of the region deformed by indentation were dependent on the material and ranged between 3a and 6a [39,40]. These values were larger than f_{e1}, indicating that the deformed region of small plastic strain did not affect the indentation results. Sudharshan Phani and Oliver [41] investigated the effect of indentation spacing on E_r and H_{it} using a Berkovich indenter and found that the elastoplastic regions of neighboring indentations were not required to obtain complete separation for reliable results. A similar observation was made in the current study.

Pile-up occurs during indentation and increases the contact area, but was not accounted for in the OP method. A parametric study using finite element analysis by Cheng and Cheng [36] and Bolshakov and Pharr [37] demonstrated that the OP method underestimates the contact area by as much as 60%. Cheng and Cheng [42] used indentation work values from finite element analysis to determine a non-dimensional function related to E_r/H_{it}. By combining this function with Eqs. (1) and (2), a modified contact area was calculated using the contact stiffness, maximum load and indentation work values. Saha et al. [43] and Kese et al. [44,45] proposed geometrical modification approaches that assumed the pile-up ridges were arc [43] and semi-ellipse [44] [45] shaped, where the ridge shape was calculated from pile-up height after unloading. This can contribute to errors, as the pile-up behavior differs between loading and unloading. The modification of the OP method is still controversial despite the proposal of numerous approaches, and the present study chose to calculate E_r using the unmodified OP method.

The estimation model assumes adiabatic heating and strain-rate sensitivity are negligibly small. A slight increase of hardness with a loading rate was reported in previous studies [46,47]. The strain-rate sensitivity remarkably appears at ultra-high strain rate [48], causing overestimation of the strain energy in the equivalent energy model. Therefore, the estimation should be performed using an indentation result at small strain rate, and one must pay attention to an estimation result when a material has high strain-rate sensitivity.

4. Inverse estimation of engineering materials

Stress-strain curves estimated from indentation results were validated using tensile testing on an aluminum-magnesium alloy (A5052) and austenitic stainless steel (SUS304) as sample materials. The indentation samples were mechanically polished and electropolished to minimize surface roughness and residual strain. Indentations were performed at $P_{max} = 1.5$ N and $dP/dt = 100$ mN/s using a Bruker TI-900 nanoindenter, followed by the measurement of pile-up topography using a Keyence VK-9700 laser microscope. The tensile tests were performed using a Shimadzu AG-X universal testing instrument with constant crosshead speed of 0.6 mm/s. The elastoplastic properties were calculated as mean values from indentation tests performed in triplicate. E_r and H_{it} values were calculated from the load-displacement curves using the OP method. The h_{pile} value was the mean maximum height, calculated from the cross-section through a vertex and center of the side of an indentation mark, and used to calculate H_p.

True stress-strain curves in Fig. 6 were based on the proposed method estimates and the tensile test measurements. The aluminum alloy fractured at $\varepsilon = 6.5\%$, thus these curves were only plotted until the fracture strain. Liu et al. [49] found that the upper limit of strain (ε_c) for the estimated curves was 20% at $\theta = 70.3°$. Therefore, the stainless steel was only estimated until ε reached 20%. The estimation results were acceptably[1] accurate with reference to tensile tests, although a small error was observed. These estimation errors were attributed to the stainless steel exhibiting bi-linear behavior and not the powered law upon which the model was based.

As mentioned in *3.4. Discussion*, the OP method underestimates contact area by 60% when pile-up occurs, corresponding to overestimation of E_r by 30% [37]. In the present work, the estimated stress-strain curves possibly include the error due to the overestimation of E_r. To evaluate the error, the estimation was performed using 1.3 times reduced E_r ($E_r^* = E_r/1.3$). The estimated stress-strain curves for E_r^* were comparable to that for E_r though σ_y increased and n decreased, as shown in Fig. 6. A 60% underestimation of contact area is the worst case scenario, and the error will be negligible in most materials, particularly in those that exhibited large strain hardening.

5. Conclusions

An inverse estimation algorithm was proposed to estimate a stress-strain curve from a single indentation test. The relationship between the elastoplastic properties and indentation results was evaluated using the equivalent energy method and exponential approximation. A parametric study of indentation was performed using finite element analysis to determine the appropriate coefficients for the proposed equation. The proposed equation provided an accurate reproduction of the simulation results and was validated using an aluminum alloy and stainless steel. The stress-strain curves estimated from the indentation tests were correlated with the tensile tests. This technique allows for the estimation of elastoplastic properties at various indentation size without exchanging the indenter and is a promising alternative for the rapid evaluation of local mechanical properties.

Data availability

The data required to reproduce these findings are available from the corresponding author upon request.

Declaration of Competing Interest

The authors declare that they have no known competing financial interests or personal relationships that could have appeared to influence the work reported in this paper.

Acknowledgments

This work was financially supported by the Amada Foundation for Metal Work Technology in Japan (No. AF-2018035-C2). The authors would like to thank Dr. Susumu Takamori, Ms. Eri Nakagawa, and Ms. Yuki Yamamoto for assistance with tensile tests, indentation, and mesh verification, respectively.

[1] Large difference is seen in the stress-strain curves estimated by various dual indenter methods as shown in Guelorget et al. [28].

References

[1] W. Oliver, G. Pharr, Measurement of hardness and elastic modulus by instrumented indentation: advances in understanding and refinements to methodology, J. Mater. Res. 19 (1) (2004) 3–20.

[2] J.-H. Kim, S. Choi, J. Lee, H.-J. Ahn, Y.-C. Kim, M.-J. Choi, D. Kwon, An indentation method for evaluation of residual stress: estimation of stress-free indentation curve using stress-independent indentation parameters, J. Mater. Res. 34 (7) (2019) 1103–1111.

[3] Q. Wang, K. Ozaki, H. Ishikawa, S. Nakano, H. Ogiso, Indentation method to measure the residual stress induced by ion implantation, Nucl. Inst. Methods Phys. Res. B 242 (2006) 88–92.

[4] R. Ginder, W. Nix, G. Pharr, A simple model for indentation creep, J. Mech. Phys. Solids 112 (2018) 552–562.

[5] H. Takagi, M. Dao, M. Fujiwara, M. Otsuka, Creep characterization of aluminum-magnesium solid-solution alloy through self-similar microindentation, Mater. Trans. 47 (8) (2006) 2006–2014.

[6] T. Man, T. Ohmura, Y. Tomota, Mechanical behavior of individual retained austenite grains in high carbon quenched-tempered steel, ISIJ Int. 59 (3) (2019) 559–566.

[7] K. Sekido, T. Ohmura, L. Zhang, T. Hara, K. Tsuzaki, The effect of interstitial carbon on the initiation of plastic deformation of steels, Mater. Sci. Eng. A 530 (2011) 396–401.

[8] W. Oliver, G. Pharr, An improved technique for determining hardness and elastic modulus using load and displacement sensing indentation experiments, J. Mater. Res. 7 (6) (1992) 1564–1583.

[9] N. Ogasawara, N. Chiba, X. Chen, A simple framework of spherical indentation for measuring elastoplastic properties, Mech. Mater. 41 (9) (2009) 1025–1033.

[10] T.-H. Pham, Q.-M. Phan, S.-E. Kim, Identification of the plastic properties of structural steel using spherical indentation, Mater. Sci. Eng. A 711 (2018) 44–61.

[11] C. Moussa, X. Hernot, O. Bartier, G. Delattre, G. Mauvoisin, Identification of the hardening law of materials with spherical indentation using the average representative strain for several penetration depths, Mater. Sci. Eng. A 606 (2014) 409–416.

[12] M. Kim, K. Marimuthu, J. Lee, H. Lee, Spherical indentation method to evaluate material properties of high-strength materials, Int. J. Mech. Sci. 106 (2016) 117–127.

[13] H. Chen, L. Cai, Theoretical model for predicting uniaxial stress-strain relation by dual conical indentation based on equivalent energy principle, Acta Mater. 121 (2016) 181–189.

[14] J. Bucaille, S. Stauss, E. Felder, J. Michler, Determination of plastic properties of metals by instrumented indentation using different sharp indenters, Acta Mater. 51 (2003) 1663–1678.

[15] Y. Cao, X. Qian, J. Lu, Z. Yao, An energy-based method to extract plastic properties of metal materials from conical indentation tests, J. Mater. Res. 20 (5) (2005) 1194–1206.

[16] N. Ogasawara, N. Chiba, X. Chen, Limit analysis-based approach to determine the material plastic properties with conical indentation, J. Mater. Res. 21 (4) (2006) 947–957.

[17] J. Luo, J. Lin, A study on the determination of plastic properties of metals by instrumented indentation using two sharp indenters, Int. J. Solids Struct. 44 (2007) 5803–5817.

[18] M.-Q. Le, A computational study on the instrumented sharp indentations with dual indenters, Int. J. Solids Struct. 45 (2008) 2818–2835.

[19] M.-Q. Le, Material characterization by dual sharp indenters, Int. J. Solids Struct. 46 (2009) 2988–2998.

[20] C. Gamonpilas, E. Busso, Characterization of elastoplastic properties based on inverse analysis and finite element modeling of two separate indenters, J. Eng. Mater. Technol. 129 (4) (2007) 603–608.

[21] M. Kim, J. Lee, F. Rickhey, H. Lee, A dual triangular pyramidal indentation technique for material property evaluation, J. Mater. Res. 30 (8) (2015) 1098–1109.

[22] H. Hyun, M. Kim, J. Lee, H. Lee, A dual conical indentation technique based on FEA solutions for property evaluation, Mech. Mater. 43 (2011) 313–331.

[23] J. Alkorta, J. Martínez-Esnaola, J.G. Sevillano, Absence of one-to-one correspondence between elastoplastic properties and sharp-indentation load-penetration data, J. Mater. Res. 20 (2) (2005) 432–437.

[24] Y.-T. Cheng, C.-M. Cheng, Can stress-strain relationships be obtained from indentation curves using conical and pyramidal indenters? J. Mater. Res. 14 (9) (1999) 3493–3496.

[25] T. Capehart, Y.-T. Cheng, Determining constitutive models from conical indentation: sensitivity analysis, J. Mater. Res. 18 (4) (2003) 827–832.

[26] N. Chollacoop, M. Dao, S. Suresh, Depth-sensing instrumented indentation with dual sharp indenters, Acta Mater. 51 (2003) 3713–3729.

[27] K. Johnson, The correlation of indentation experiments, J. Mech. Phys. Solids 18 (1970) 115–126.

[28] B. Guelorget, M. François, C. Liu, J. Lu, Extracting the plastic properties of metal materials from microindentation tests: experimental comparison of recently published methods, J. Mater. Res. 22 (6) (2007) 1512–1519.

[29] J. Kang, A.B.W. Wen, W. Sun, Extracting elastic-plastic properties from experimental loading-unloading indentation curves using different optimization techniques, Int. J. Mech. Sci. 144 (2018) 102–109.

[30] K. Goto, I. Watanabe, T. Ohmura, Determining suitable parameters for inverse estimation of plastic properties based on indentation marks, Int. J. Plast. 116 (2019) 81–90.

[31] L. Meng, P.B.B. Raghavan, G. Mauvoisin, O. Bartier, X. Hernot, On the study of mystical materials identified by indentation on power law and voce hardening solids, Int. J. Mater. Form. 12 (2019) 587–602.

[32] C. Moy, M. Bocciarelli, S. Ringer, G. Ranzi, Identification of the material properties of Al 2024 alloy by means of inverse analysis and indentation tests, Mater. Sci. Eng. A 529 (2011) 119–130.

[33] G. Bolzon, B. Molinas, M. Talassi, Mechanical characterization of metals by indentation tests: an experimental verification study for on-site applications, Strain 48 (2012) 517–527.

[34] A. Atkins, D. Tabor, Plastic indentation in metals with cones, J. Mech. Phys. Solids 13 (1965) 149–164.

[35] N. Ogasawara, N. Chiba, X. Chen, Representative strain of indentation analysis, J. Mater. Res. 20 (8) (2005) 2225–2234.

[36] Y.-T. Cheng, C.-M. Cheng, Effects of 'sinking in' and 'pilling up' on estimating the contact area under load in indentation, Philos. Mag. Lett. 78 (2) (1998) 115–120.

[37] A. Bolshakov, G. Pharr, Influences of pileup on the measurement of mechanical properties by load and depth sensing indentation techniques, J. Mater. Res. 13 (4) (1998) 1049–1058.

[38] M. Ashby, D. Jones, Engineering Materials, 4 ed. Butterworth-Heinemann, Oxford, 2013.

[39] E. Hintsala, U. Hangen, D. Stauffer, High-throughput nanoindentation for statistical and spatial property determination, JOM 70 (4) (2018) 494–503.

[40] L. Samuels, T. Mulhearn, An experimental investigation of the deformed zone associated with indentation hardness impressions, J. Mech. Phys. Solids 5 (1957) 125–134.

[41] P.S. Phani, W. Oliver, A critical assessment of the effect of indentation spacing on the measurement of hardness and modulus using instrumented indentation testing, Mater. Des. 164 (2019) 107563.

[42] Y.-T. Cheng, C.-M. Cheng, Relationships between hardness, elastic modulus, and the work of indentation, Appl. Phys. Lett. 73 (5) (1998) 614–616.

[43] R. Saha, W. Nix, Soft films on hard substrates—nanoindentation of tungsten films on sapphire substrates, Mater. Sci. Eng. A 319–321 (2001) 898–901.

[44] K. Kese, Z. Li, B. Bergman, Method to account for true contact area in soda-lime glass during nanoindentation with the Berkovich tip, Mater. Sci. Eng. A 404 (2005) 1–8.

[45] K. Kese, Z. Li, Semi-ellipse method for accounting for the pile-up contact area during nanoindentation with the Berkovich indenter, Scr. Mater. 55 (2006) 699–702.

[46] J. Chen, Y. Shen, W. Liu, B. Beake, X. Shi, Z. Wang, Y. Zhang, X. Guo, Effects of loading rate on development of pile-up during indentation creep of polycrystalline copper, Mater. Sci. Eng. A 656 (2016) 216–221.

[47] V. Maier-Kiener, K. Durst, Advanced nanoindentation testing for studying strain-rate sensitivity and activation volume, JOM 69 (11) (2017) 2246–2255.

[48] P. Phani, W. Oliver, Ultra high strain rate nanoindentation testing, Materials 10 (6) (2017) 663.

[49] L. Liu, N. Ogasawara, N. Chiba, X. Chen, Can indentation technique measure unique elastoplastic properties? J. Mater. Res. 24 (3) (2009) 784–800.